J|A|C|S
ARTICLES

Published on Web 07/20/2009

Scalable Synthesis of Few-Layer Graphene Ribbons with Controlled Morphologies by a Template Method and Their Applications in Nanoelectromechanical Switches

Dacheng Wei, Yunqi Liu,* Hongliang Zhang, Liping Huang, Bin Wu, Jianyi Chen, and Gui Yu

Beijing National Laboratory for Molecular Sciences, Institute of Chemistry, Chinese Academy of Sciences, Beijing 100190, People's Republic of China

Received April 17, 2009; E-mail: liuyq@iccas.ac.cn

Abstract: Controllable and scalable production is of great importance for the application of graphene; however, to date, it is still a great challenge and a major obstacle which hampers its practical applications. Here, we develop a template chemical vapor deposition method for scalable synthesis of few-layer graphene ribbons (FLGRs) with controlled morphologies. The FLGRs have a good conductivity and are ideal for use in nanoelectromechanics (NEM). As an application, we fabricate a reversible NEM switch and a logic gate by using the FLGRs. This work realizes both controllable and scalable synthesis of graphene, provides an application of graphene in NEM switches, and would be valuable for both the scientific studies and the practical applications of graphene.

1. Introduction

Graphene, a newly discovered material with carbon atoms parked in a two-dimensional honeycomb lattice,[1] has attracted great attention of both experimental and theoretical scientists in recent years,[2] as this material combines excellent mechanical and electrical properties with atomic thickness, which makes it one of the most promising candidates for future nanoelectronics[3] and holds great promise for widespread applications such as sensors, nanocomposites, supercapacitors, and hydrogen storage.[2] As the first step to realize these applications, graphene must be synthesized in large scale with controlled morphologies, thus the controllable and scalable production is of great importance for its applications. To date, mechanical exfoliation,[1] thermal decomposition of SiC,[4] oxidation of graphite,[5] and liquid-phase exfoliation of graphite[6,7] have been developed to produce single-layer or few-layer graphene; however, the morphologies are still hard to control by these methods due to the random exfoliation or growth process. Very recently, Dai et al. and Tour et al. successfully produced graphene nanoribbons by plasma etching of carbon nanotubes partly embedded in a polymer film[8] or by lengthwise cutting and unraveling of multiwalled carbon nanotube side walls.[9] Chemical vapor deposition (CVD) is a general method for controllably producing various types of nanomaterials,[10] and several groups have demonstrated the patterned growth of few-layer graphene on chips by CVD;[11−13] however, scaling up of the patterned growth is still limited in success due to the limit surface of the chips. Therefore, although great efforts have been made, scalable production of graphene with well-controlled morphologies is still a great challenge and a major obstacle which hampers practical applications of graphene.

One significant potential application of graphene is in nanoelectromechanics (NEM),[14] as graphene not only shows excellent electronic properties but also has atomic thickness, large surface area, low mass density, high stiffness, and enormous strength.[15,16] Since the 1990s, much attention to NEM has been attracted by carbon nanotubes, a seamless rolled-up

(1) Novoselov, K. S.; Geim, A. K.; Morozov, S. V.; Jiang, D.; Zhang, Y.; Dubonos, S. V.; Grigorieva, I. V.; Firsov, A. A. *Science* **2004**, *306*, 666–669.
(2) (a) Geim, A. K.; Novoselov, K. S. *Nat. Mater.* **2007**, *6*, 183–191. (b) Katsnelson, M. I. *Mater. Today* **2007**, *10*, 20–27.
(3) Areshkin, D. A.; White, C. T. *Nano Lett.* **2007**, *7*, 3253–3259.
(4) Berger, C.; et al. *Science* **2006**, *312*, 1191–1196.
(5) Dikin, D. A.; Stankovich, S.; Zimney, E. J.; Piner, R. D.; Dommett, G. H. B.; Evmenenko, G.; Nguyen, S. T.; Ruoff, R. S. *Nature* **2007**, *448*, 457–460.
(6) Li, X. L.; Wang, X. R.; Zhang, L.; Lee, S. W.; Dai, H. J. *Science* **2008**, *319*, 1229–1232.
(7) (a) Li, X. L.; Zhang, G. Y.; Bai, X. D.; Sun, X. M.; Wang, X. R.; Wang, E. G.; Dai, H. J. *Nat. Nanotechnol.* **2008**, *3*, 538–542. (b) Hernandez, Y. *Nat. Nanotechnol.* **2008**, *3*, 563–568. (c) Choucair, M.; Thordarson, P.; Stride, J. A. *Nat. Nanotechnol.* **2009**, *4*, 30–33.
(8) Jiao, L. Y.; Zhang, L.; Wang, X. R.; Diankov, G.; Dai, H. J. *Nature* **2009**, *458*, 877–880.
(9) Kosynkin, D. V.; Higginbotham, A. L.; Sinitskii, A.; Lomeda, J. R.; Dimiev, A.; Price, B. K.; Tour, J. M. *Nature* **458**, 872–876.
(10) (a) Xia, Y.; Yang, P.; Sun, Y.; Wu, Y.; Mayers, B.; Gates, B.; Yin, Y.; Kim, F.; Yan, H. *Adv. Mater.* **2003**, *15*, 353–389. (b) Wei, D. C.; Liu, Y. Q.; Cao, L. C.; Fu, L.; Li, X. L.; Wang, Y.; Yu, G. *J. Am. Chem. Soc.* **2007**, *129*, 7364–7368. (c) Wei, D. C.; Cao, L. C.; Fu, L.; Li, X. L.; Wang, Y.; Yu, G.; Liu, Y. Q. *Adv. Mater.* **2007**, *19*, 386–390.
(11) Di, C. A.; Wei, D. C.; Yu, G.; Liu, Y. Q.; Guo, Y. L.; Zhu, D. B. *Adv. Mater.* **2008**, *20*, 3289–3293.
(12) Kim, K. S.; Zhao, Y.; Jang, H.; Lee, S. Y.; Kim, J. M.; Kim, H. S.; Ahn, J. H.; Kim, P.; Choi, J. Y.; Hong, B. H. *Nature* **2009**, *457*, 706–710.
(13) Reina, A.; Jia, X.; Ho, J.; Nezich, D.; Son, H.; Bulovic, V.; Dresselhaus, M. S.; Kong, J. *Nano Lett.* **2009**, *9*, 30–35.
(14) (a) Garcia-Sanchez, D.; van der Zande, A. M.; San Paulo, A.; Lassange, B.; McEuen, P. L.; Bachtold, A. *Nano Lett.* **2008**, *8*, 1399–1403. (b) Bunch, J. S.; van der Zande, A. M.; Verbridge, S. S.; Frank, L. W.; Tanenbaum, D. M.; Parpia, J. M.; Craighead, H. G.; McEuen, P. L. *Science* **2007**, *315*, 490–493.

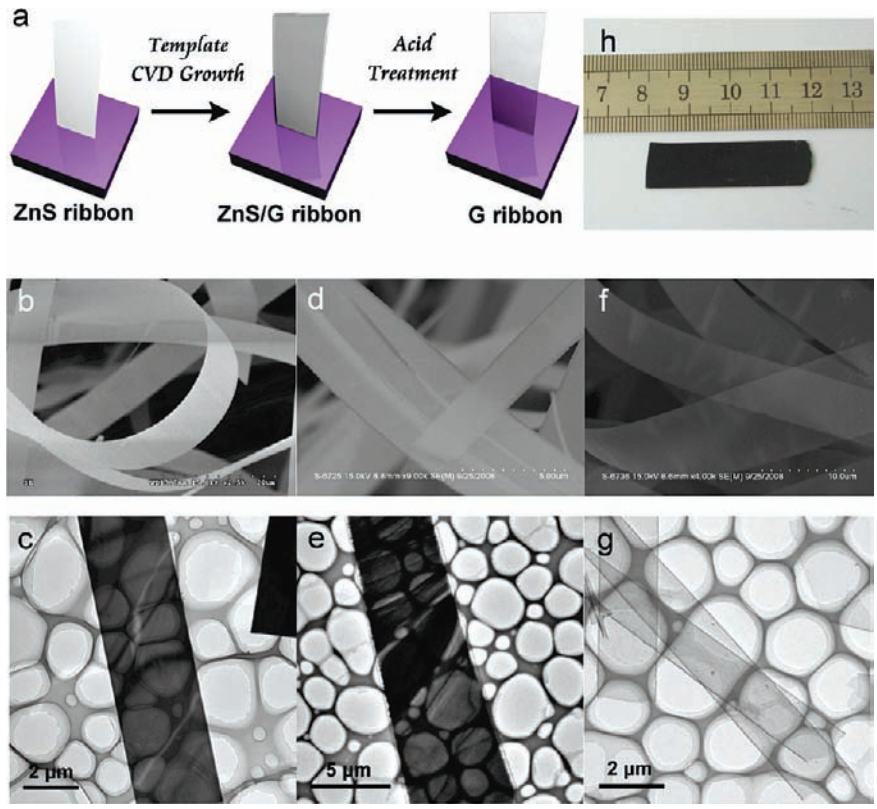

Figure 1. (a) Schematic diagram of the template CVD growth of the FLGRs. (b−g) SEM images (b,d,f) and TEM images (c,e,g) of the ZnS ribbons (b,c), the ZnS/G ribbons (d,e), and the FLGRs (f,g). (h) Photo image of the FLGRs grown on a Si substrate.

graphene sheet, and various types of NEM devices have been demonstrated based on carbon nanotubes.[17] Only recently, pioneering work on graphene has been performed by McEuen et al.,[14] in which NEM resonators have been fabricated by using single-layer and few-layer graphene sheets. Here, we develop a template CVD method to produce few-layer graphene ribbons (FLGRs) for the first time and demonstrate a reversible NEM switch device based on them. The template CVD growth realizes both scalable production and control of the morphologies. The produced FLGRs exhibit a good conductivity and are ideal for use in NEM switches, resulting in a good reversible switching behavior and an on/off ratio in the range of 10^4-10^8. Moreover, as an application, a logic OR gate is fabricated by using these NEM switches.

2. Experimental Section

Synthesis. The experimental setup is shown in Figure S1 in the Supporting Information. In a typical experiment, first, ZnS ribbons were produced on a Si substrate by a physical vapor deposition (PVD) method using Au as the catalyst (see details in Supporting Information). Then, the Si substrate with the produced ZnS ribbons was placed at the center of a horizontal quartz tube mounted inside a high-temperature furnace. Before heating, 150 sccm Ar and 150 sccm H_2 were introduced for 30 min to remove the air, and then 50 sccm Ar and 50 sccm H_2 were introduced as the carrier gas. When the center of the furnace reached 750 °C, 100 sccm CH_4 (>99.9%) was introduced as the carbon source. This process lasted for 8 min, and then CH_4 was turned off and the furnace was cooled to room temperature under ambient H_2. To obtain the FLGRs, the Si substrate with the produced ZnS/G ribbons was immerged in 0.1 M HCl for 30 min and then was washed by distilled water. After drying the sample at 120 °C for 2 h, the FLGRs were obtained on the whole surface of the Si substrate.

Characterization. The samples were characterized by using scanning electron microscopy (SEM, Hitachi S-4300, operated at 15 kV), transmission electron microscopy (TEM, Hitachi-2010, operated at 200 kV) equipped with an X-ray energy dispersive spectrometer (EDS), X-ray diffractometer (XRD, Rigaku Dmax2000, Cu Kα), X-ray photoelectron spectroscopy (XPS, ESCA Lab220I-XL), Raman spectroscopy (LabRam HR800 with laser excitation at 633 nm), and atomic force microscopy (AFM, tapping mode, Innova Microscope, Veeco Instruments Inc., USA).

Device and Electrical Measurement. To transfer the FLGRs onto electrodes, the FLGRs were scratched from the Si substrate and dispersed in ethanol by mild sonication, and then the solution was dripped on a 500 nm thick thermally oxidized Si surface with Au/Ti contact pads. After drying, a single FLGR could be found to bridge the neighboring Au/Ti pads by SEM. To obtain better contact, the device was annealed at 300 °C in Ar for 15 min. Finally, a NEM switch device was obtained after cutting the FLGR by current breakdown. The electrical measurement was performed by using a probe station (Wentworth Company MP1008) and a semiconductor parameter analyzer (Keithley Instruments Inc. 4200) at room temperature in air.

3. Results and Discussion

FLGRs were synthesized via a template CVD method illustrated in Figure 1. First, ZnS ribbons, which acted as the

(15) (a) Lee, C. G.; Wei, X. D.; Kysar, J. W.; Hone, J. *Science* **2008**, *321*, 385–388. (b) Frank, I. W.; Tanenbaum, D. M.; van der Zande, A. M.; McEuen, P. L. *J. Vac. Sci. Technol., B* **2007**, *25*, 2558–2561.
(16) Poot, M.; van der Zant, H. S. J. *Appl. Phys. Lett.* **2008**, *92*, 063111.
(17) (a) Kim, P.; Lieber, C. M. *Science* **1999**, *286*, 2148–2150. (b) Rueckes, T.; Kim, K.; Joselevich, E.; Tseng, G. Y.; Cheung, C. L.; Lieber, C. M. *Science* **2000**, *289*, 94–97. (c) Sazonova, V.; Yaish, Y.; Ustunel, H.; Roundy, D.; Arias, T. A.; McEuen, P. L. *Nature* **2004**, *431*, 284–287. (d) Jang, J. E.; Cha, S. N.; Choi, Y. J.; Kang, D. J.; Butler, T. P.; Hasko, D. G.; Jung, J. E.; Kim, J. M.; Amaratunga, G. A. J. *Nat. Nanotechnol.* **2008**, *3*, 26–30.

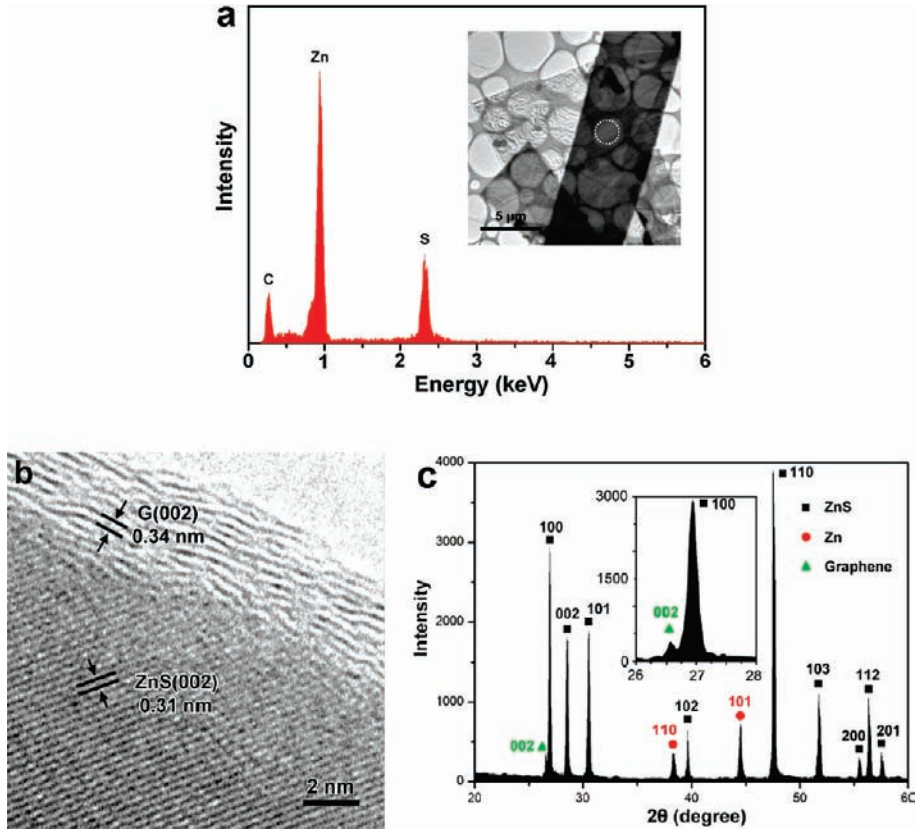

Figure 2. (a) EDS spectrum, (b) HRTEM image, and (c) XRD pattern of the ZnS/G ribbons. Inset of (a) is a TEM image, in which the EDS spectrum is taken from the area marked by the dashed cycle.

template and the catalyst for growth of the graphene ribbons, were prepared in large scale on Si substrates by a PVD process. SEM (Figures 1b and S2 in Supporting Information) and TEM (Figures 1c and S3 in Supporting Information) images show that the ZnS ribbons have a uniform morphology with an average width of 0.5−5 μm and a length of tens to several hundred micrometers. The selected-area electron diffraction (SAED) pattern (Figure S3 in Supporting Information) reveals that they are single crystalline with a perfect wurtzite structure. Second, after an 8 min CVD growth by using 100 sccm CH_4 as the carbon source, a uniform carbon layer was deposited on the surface of the ZnS ribbons. As shown in SEM images (Figures 1d and S3 in Supporting Information), almost all of the ZnS ribbons are completely coated by a uniform sheet with light contrast along their total length, and this uniform configuration can be confirmed by TEM characterization (Figure 1e). EDS spectrum (Figure 2a) reveals the ribbons are composed of Zn, S, and C elements, confirming the deposit of C on the ZnS ribbons. High-resolution TEM (HRTEM) image (Figure 2b) and XRD pattern (Figure 2c) reveal that both the ZnS ribbons and the deposited carbon are well crystallized. In the XRD pattern, the sharp diffraction peaks with relatively high intensity can be clearly indexed as the wurtzite ZnS phase (JCPDS No. 36-1450), while the weak reflection peaks can be indexed to the crystalline graphitic carbon (JCPDS No. 26-1076) and the hexagonal Zn (JCPDS No. 4-831). The HRTEM image of a ZnS/graphene (ZnS/G) ribbon confirms that the deposited carbon is graphitic with about 10 layers. Finally, after removing ZnS by HCl treatment, graphene ribbons were obtained. The wide survey XPS (Figure S4 in Supporting Information) spectrum of the product shows the predominant presence of C, and the main peak (Figure 3a) is located at 284.8 eV, corresponding to the graphite-like sp^2 C, thus most of the C atoms are arranged in a conjugated honeycomb lattice. SEM (Figure 1f) and TEM (Figure 1g) images show that the products are graphene ribbons with a shape similar to the ZnS ribbons, and a very tiny amount of carbon nanotubes can also be observed occasionally in some cases. The graphene ribbons are uniform along their total length, thus the morphologies of the graphene ribbons can be defined and well controlled by the ZnS ribbons. The uniform graphene ribbons are obtained on the whole surface of the Si substrate (Figures 1h and S5 in Supporting Information), thus the template CVD growth is large scale and has the potential to be further scaled up by using larger substrates.

According to the layer number, graphene can be distinguished as single-layer or few-layer graphene. As observed from the HRTEM image (Figure 3b), the graphene ribbons, produced here, are predominantly the few-layer graphene with about 10 graphitic layers. Raman spectrum (633 nm) of the graphene ribbons (Figure 3c) reveals the presence of D, G, and 2D bands, located at ca. 1329, 1591, and 2652 cm^{-1}, respectively. The D band, which only occurs in the sp^2 C with defects,[18] would originate from the edges and the subdomain boundaries of graphene layers in our case.[13] The 2D band is the most prominent feature in the Raman spectrum of graphene, and its shape is highly sensitive to identify single-layer graphene and few-layer graphene.[19] In case of the single-layer graphene, the 2D band is a single, symmetric, and very sharp peak at lower frequency, while the few-layer graphene has a broader 2D band due to the change of electronic structure of graphene, which affects the process of double resonance.[18,20] In the case of the graphite, the higher frequency components of the 2D band

(18) Thomsen, C.; Reich, S. *Phys. Rev. Lett.* **2000**, *85*, 5214–5217.

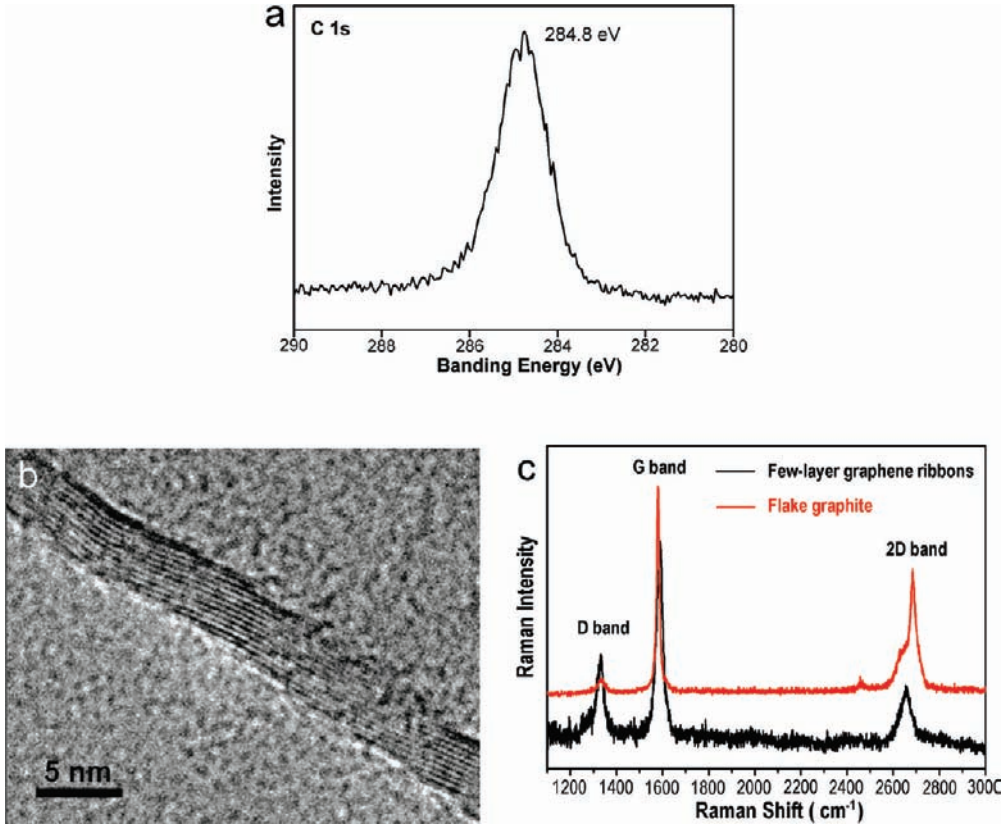

Figure 3. (a,b) XPS C1s spectrum (a) and HRTEM image (b) of the FLGRs. (c) Raman spectra (633 nm) of the FLGRs and the flake graphite.

increase compared with the few-layer graphene, as further increasing graphitic layers will lead to a significant decrease of the relative intensity of the lower frequency component.[19] In our case, the 2D band is a wide peak at 2652 cm^{-1}, while the flake graphite has a wider peak at 2688 cm^{-1}, thus our products are few-layer graphene, consistent with the HRTEM characterization.

The thickness of the produced few-layer graphene sheet can be controlled by the growth time and the flow rate of CH_4 in the CVD process. The graphene sheet is about 3.4 nm thick with about 10 graphitic layers after 8 min growth in 100 sccm CH_4 (Figure 4a). After a shorter growth time of 4 min in 100 sccm CH_4, the thickness decreases to about 2.2 nm (Figure 4b); however, if the growth lasts for a longer time of 20 min in 100 sccm CH_4, some ZnS core is evaporated, although the thickness increases (Figure 4c). The flow rate of CH_4 can also effectively control the thickness. At a lower flow rate of 30 sccm CH_4 (Figure 4d) and 60 sccm CH_4 (Figure 4e), the thickness decreases to about 1.7 and 2.5 nm after 8 min growth, while thicker few-layer graphene sheet of about 6.7 nm can be produced at a higher flow rate of 200 sccm CH_4 (Figure 4f).

To observe the detailed structure of the FLGRs, we measured their open ends by AFM. The FLGR sample, used here, was produced for 4 min in 30 sccm CH_4 to obtain thin FLGRs. HRTEM images (Figure 5a,b) of the sample before and after removing ZnS show that the graphene sheets have about 4−5 graphitic layers. After HCl treatment, the FLGRs were transferred to quartz substrates for AFM characterization. AFM image (Figure 5c) of an open end of a FLGR shows that the FLGR has a bilayer looping structure with closed folding edges and two few-layer graphene sheets closely attached with each other. The total height of the FLGR is about 4.92 nm, while the bottom few-layer graphene sheet of the FLGR is about 2.19 nm in height. Height measurements extracted from a series of AFM images show that the total thickness of the FLGRs ranges from 4.5 to 7.5 nm. In fact, this structure was also observed by Gogotsi et al.,[21] Liu et al.,[22] and Campos-Delgado et al.[23] after thermal annealing of the graphenes with open edges. They found that the adjacent graphitic layers were more likely to join their edges to form the bilayer looping structure with closed folding edges at very high temperature because of the reduced number of dangling bonds.

In normal routes, graphene was produced by the mechanical or liquid-phase exfoliation of graphite, and Dai et al. have successfully produced the graphene nanoribbons by high-temperature exfoliation;[11] however, the nanoribbons show various shapes due to the random exfoliation process. Comparatively, CVD is controllable for producing various types of nanomaterials, and in the case of graphene, transition metals such as Co, Pt, Ir, Ru, Cu, and Ni are used as the catalyst for the CVD growth of graphene,[11−13,24,25] and patterning of the metals realizes patterned CVD growth of graphene;[11−13] however, limited surface hampers its scaling up. Recently, bulk

(19) (a) Ferrari, A. C.; et al. *Phys. Rev. Lett.* **2006**, *97*, 187401. (b) Graf, D.; Molitor, F.; Ensslin, K.; Stampfer, C.; Jungen, A.; Hierold, C.; Wirtz, L. *Nano Lett.* **2007**, *7*, 238–242.
(20) Ni, Z. H.; Wang, H. M.; Kasim, J.; Fan, H. M.; Yu, T.; Wu, Y. H.; Feng, Y. P.; Shen, Z. X. *Nano Lett.* **2007**, *7*, 2758–2763.
(21) Gogotsi, Y.; Libera, J. A.; Kalashnikov, N.; Yoshimura, M. *Science* **2000**, *290*, 317–320.
(22) Liu, Z.; Suenaga, K.; Harris, P. J. F.; Iijima, S. *Phys. Rev. Lett.* **2009**, *102*, 015501.
(23) Campos-Delgado, J.; et al. *Chem. Phys. Lett.* **2009**, *469*, 177–182.
(24) (a) Coraux, J.; Ndiaye, A. T.; Busse, C.; Michely, T. *Nano Lett.* **2008**, *8*, 565–570. (b) de Parga, A. L. V.; Calleja, F.; Borca, B.; Passeggi, J. M. C. G.; Hinarejos, J. J.; Guinea, F.; Miranda, R. *Phys. Rev. Lett.* **2008**, *100*, 056807. (c) Ueta, H.; Saida, M.; Nakai, C.; Yamada, Y.; Sasaki, M.; Yamamoto, S. *Surf. Sci.* **2004**, *560*, 183–190.

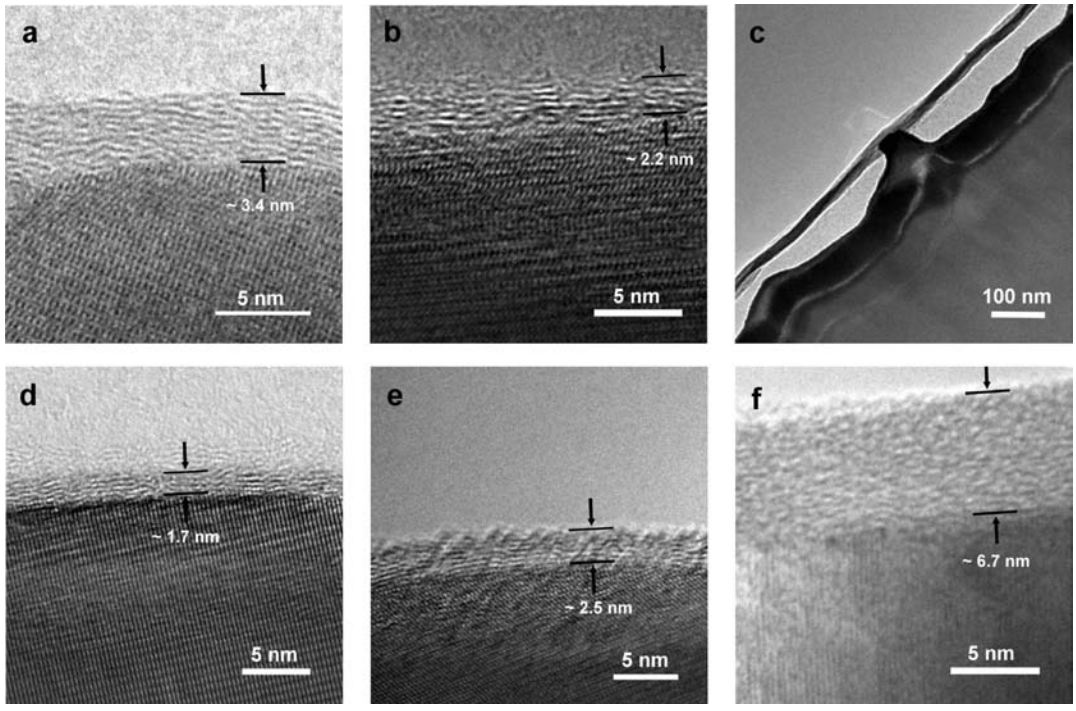

Figure 4. (a−c) HRTEM or TEM images of the ZnS/G ribbons grown in 100 sccm CH_4 for 8 min (a), 4 min (b), and 20 min (c). (d−f) HRTEM images of the ZnS/G ribbons grown for 8 min in 30 sccm CH_4 (d), 60 sccm CH_4 (e), and 200 sccm CH_4 (f).

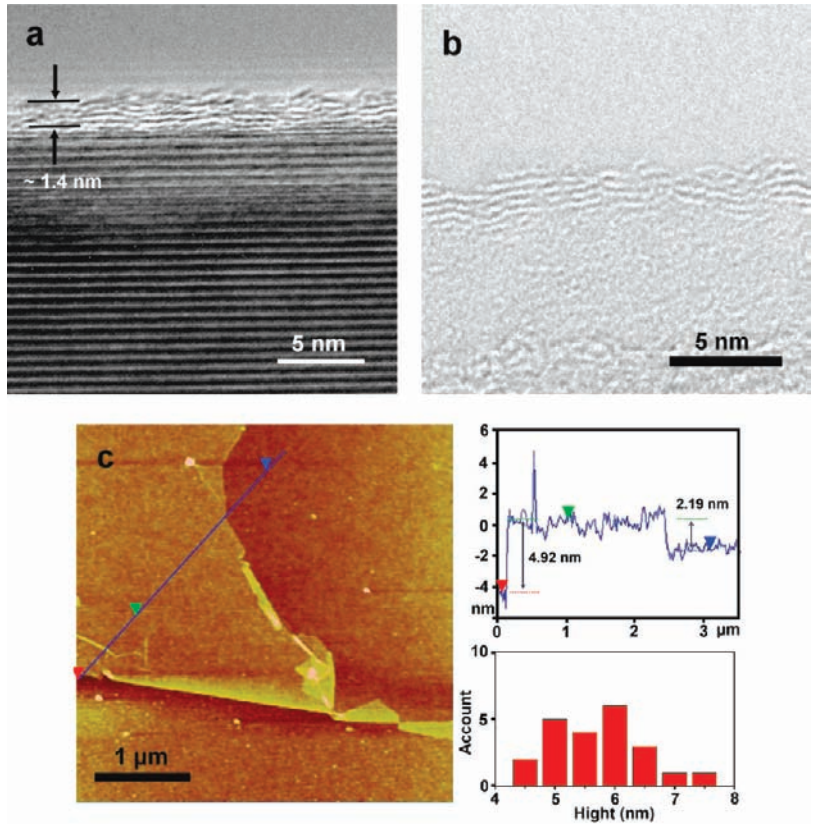

Figure 5. (a) HRTEM image of a ZnS/G ribbon grown in 30 sccm CH_4 for 4 min. (b) HRTEM image of a FLGR after removing ZnS. (c) AFM image of an open end of a FLGR. Upper inset is the topography height profile along the blue line in the AFM image. Lower inset shows the distribution of the total thickness of the FLGRs.

samples of graphene ribbons have been obtained by CVD in the presence of Fe and S;[26] however, a manner is absent in the growth to well define their morphologies. Template method is a controllable and scalable route for many other types of nanomaterials.[27] In our case, the ZnS ribbons serve as both the template and the catalyst for growth of the graphene ribbons. In the growth, the surface of the ZnS ribbons is reduced to Zn by H_2 at high temperature, which can be observed from the XRD characterization (Figure 2c). As Zn can catalyze the growth of carbon nanotubes,[28] CH_4 will decompose and dissolve in Zn,

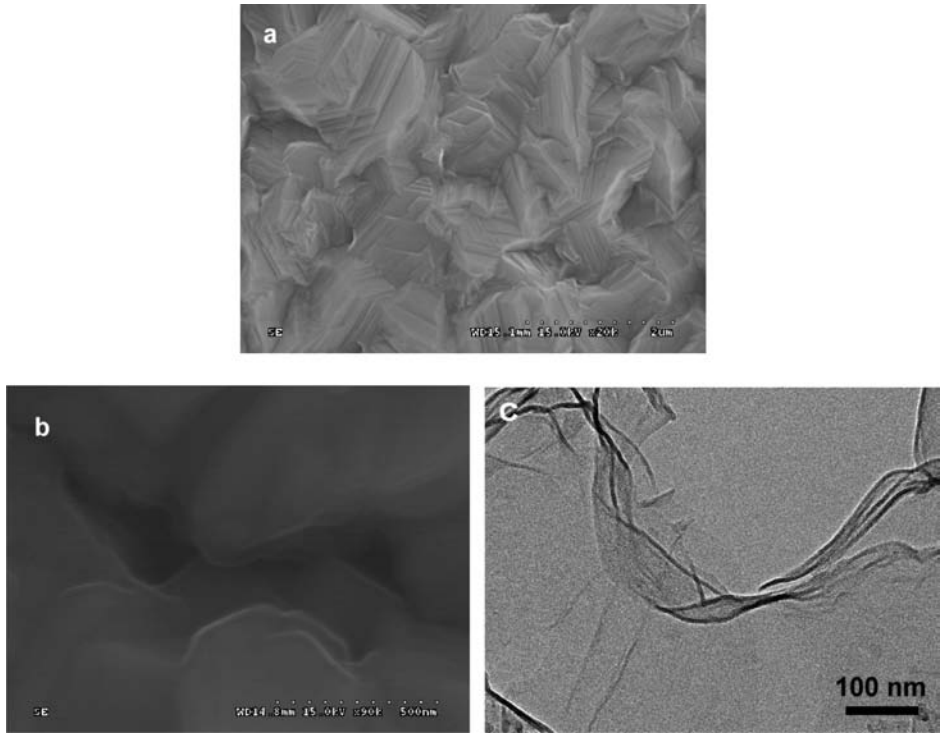

Figure 6. SEM images of a ZnS film before (a) and after (b) growth of the graphene membrane on it. (c) TEM image of a graphene membrane after HCl treatment.

and then graphitic carbon layers grow from the saturated Zn by means of precipitation. Besides the ZnS ribbons, we also realized production of graphene membranes on the ZnS films (Figure 6; see details in Supporting Information), thus ZnS catalyzes the growth of graphene. As the growth occurs on the surface of ZnS, hollow structures of graphene form outside of the ZnS ribbons. After removing the ZnS ribbons, the hollow structures of graphene tend to collapse and then form a ribbon-like structure because of a $\pi-\pi$ stacking interaction. The $\pi-\pi$ stacking interaction exists in various types of sp^2 carbon nanostructures, which causes the formation of the bundle structures of single-walled carbon nanotubes. In the case of graphene, researchers found that the $\pi-\pi$ stacking interaction could cause the agglomerate of graphene sheets in suspension[29] and the rolling of the graphene nanoribbons.[30,31] In our case, the foreside and backside few-layer graphene sheets would like to closely attach with each other and then form a bilayer looping structure of FLGRs due to the $\pi-\pi$ stacking interaction. As the growth of graphene takes place on the surface of the ZnS ribbons, the ZnS ribbons serve as the template and the morphologies of the graphene ribbons are well-defined. Due to the large surface area of the ZnS ribbons, scalable growth of the graphene ribbons is realized. Furthermore, besides CH_4, we also used other organic molecules, such as 50 sccm C_2H_2 (Figure S6a in Supporting Information), iron(II) phthalocyanine (Figure S6b in Supporting Information), and C_2H_5OH (Figure S6c in Supporting Information), as the carbon source in the CVD process and successfully produced the FLGRs.

To measure the electrical properties, we dispersed the FLGRs between the Au/Ti electrodes on a SiO_2/Si substrate (Figures 7a and S7 in Supporting Information) and then annealed at 300 °C in Ar to obtain better contact. AFM image of a resulting FLGR device (Figure S8 in Supporting Information) shows that the height of the electrodes is about 110 nm, and the FLGR does not suspend on the electrodes but attaches the SiO_2/Si substrate. Typical current−voltage ($I-V$) curves at different back gate voltage (V_g) and a typical transfer curve are shown in Figure 7b and Figure S9 in Supporting Information, respectively. For all the $I-V$ measurements, a linear behavior is observed, indicating a good ohmic contact with the Au/Ti electrodes, and the graphene ribbons exhibit a good conductivity and a poor V_g modulation with a Dirac point at about 25 V, thus the ribbons behaved like a metal, which would originate from the zero band gap of graphene.[2]

As an application, we fabricated the NEM switches of FLGRs by current breakdown. We applied a bias on the graphene ribbon and gradually ramped up the bias voltage while monitoring the current. At a critical voltage of approximately 12 V, the measured current dropped precipitously, down to the noise limit of the electrical measurement (inset of Figure 7b). SEM image (Figure 8a) shows that the ribbon has been completely cut, and the fracture faces are curled, forming a gap with about 30−200 nm in width and about 9 μm in length. Figure 8b shows an $I-V$ curve of the device after current breakdown. At low bias region (<7 V), the current is very low, about $10^{-13}-10^{-9}$ A, corresponding to the "OFF" state. If the bias increases over a threshold voltage (V_t) of ca. 7 V, the current sharply increases by about 4 orders of magnitude to 4×10^{-6} A, corresponding to the "ON" state. The sharp increase of current means that a small difference in bias can switch the current, leading to low

(25) Wei, D. C.; Liu, Y. Q.; Wang, Y.; Zhang, H. L.; Huang, L. P.; Yu, G. *Nano Lett.* **2009**, *9*, 1752–1758.
(26) Campos-Delgado, J.; et al. *Nano Lett.* **2008**, *8*, 2773–2778.
(27) (a) Li, J.; Papadopoulos, C.; Xu, J. *Nature* **1999**, *402*, 253. (b) Meng, G. W.; Jung, Y. J.; Cao, A. Y.; Vajtai, R.; Ajayan, P. M. *Proc. Natl. Acad. Sci. U.S.A.* **2005**, *102*, 7074–7078.
(28) Liu, J. W.; Li, X. J.; Dai, L. M. *Adv. Mater.* **2006**, *18*, 1740–1744.
(29) Seger, B.; Kamat, P. V. *J. Phys. Chem. C* **2009**, *113*, 7990–7995.
(30) Yu, D.; Liu, F. *Nano Lett.* **2007**, *7*, 3046–3050.
(31) Xie, X.; Ju, L.; Feng, X. F.; Sun, Y. H.; Zhou, R. F.; Liu, K.; Fan, S. S.; Li, Q. Q.; Jiang, K. L. *Nano Lett.* **2009**, *9*, 2565−2570.

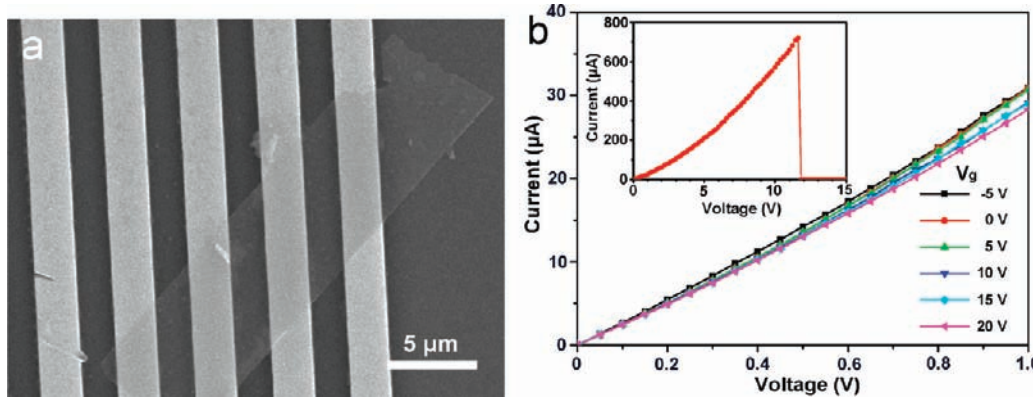

Figure 7. (a) SEM image of a FLGR device. (b) $I-V$ curves of the FLGR device at different V_g. The inset is the $I-V$ curve of a FLGR device in the current breakdown process.

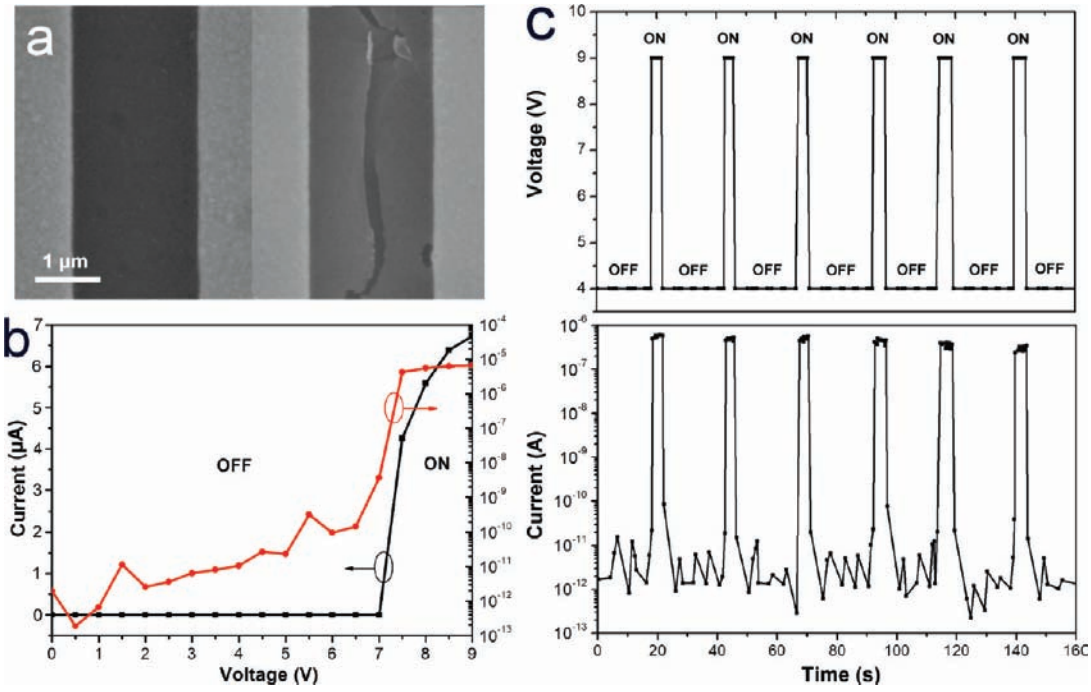

Figure 8. (a) SEM images of a FLGR device before (left) and after (right) current breakdown. (b) $I-V$ curve of the resulting NEM switch. (c) Reversible switching of a NEM switch device between "ON" and "OFF" states as the bias is cycled at 4 and 9 V.

power consumption.[32] Therefore, the device behaves as a bias-dependent switch, which can be switched between "ON" and "OFF" states by applying a bias higher or lower than V_t. We repeatedly cycled the bias of a FLGR switch below (4 V) and above (9 V) V_t, and a good reversible switching behavior was observed (Figure 8c) with an on/off ratio of about 10^5. We fabricated more than 30 devices. V_t was different for each device; however, almost all devices showed similar reversible switching behavior with on/off ratios ranging from 10^4 to 10^8.

The reversible switching behavior should originate from a NEM process, as illustrated in Figure 9. The breakdown of FLGRs can introduce topological defects in the graphitic lattice near the fracture faces,[33] which could create the curvature of the graphitic sheet,[34,35] thus the fracture edges are curled, and then a long, narrow nanogap is formed within the graphene ribbon, which acts as the responsible component for the reversible switching behavior. This configuration can be regarded as a nanoscale capacitor with air dielectric. When a bias is applied across the gap, opposite electrostatic charges are induced on the opposite curled edges, giving rise to an electrostatic attractive force (F_a) on both curled edges to deflect them toward each other. In the case of an ideal parallel plate capacitor, F_a can be calculated as

$$F_a = \varepsilon S V^2/d^2 \quad (1)$$

where ε is the dielectric constant, S is the plate area, V is the bias, and d is the gap width between plates. According to eq 1,

(32) Jang, J. E.; Cha, S. N.; Choi, Y. J.; Kang, D. J.; Butler, T. P.; Hasko, D. G.; Jung, J. E.; Kim, G. J. M.; Amaratunga, A. J. *Nat. Nanotechnol.* **2008**, *3*, 26–30.
(33) (a) Kaxiras, E.; Pandey, K. C. *Phys. Rev. Lett.* **1988**, *61*, 2693–2696. (b) Chiu, H. Y.; Deshpande, V. V.; Postma, H. W. C.; Lau, C. N.; Miko, C.; Forro, L.; Bockrath, M. *Phys. Rev. Lett.* **2005**, *95*, 226101.
(34) Andriotis, A. N.; Menon, M.; Srivastava, D.; Chernozatonskii, L. *Phys. Rev. Lett.* **2001**, *87*, 066802.
(35) (a) Scuseria, G. E. *Chem. Phys. Lett.* **1992**, *195*, 534. (b) Lee, G. D.; Wang, C. Z.; Yu, J. J.; Yoon, E.; Hwang, N. M.; Ho, K. M. *Phys. Rev. B* **2007**, *76*, 165413.

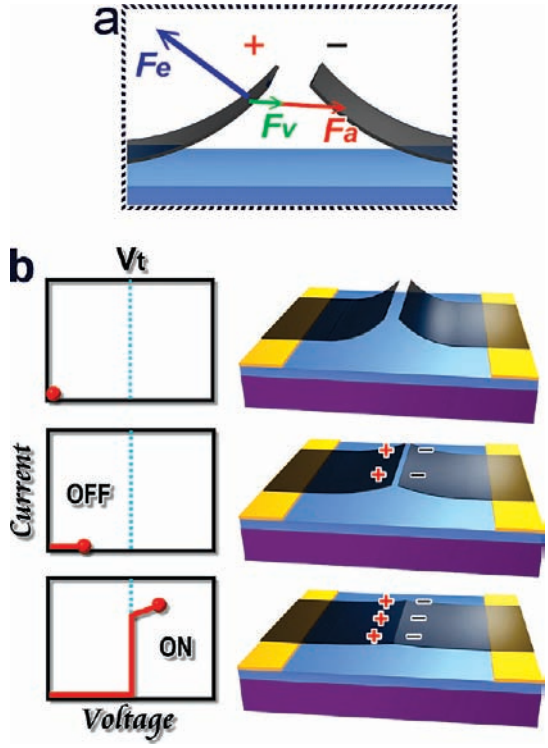

Figure 9. (a) Schematic illustration of the forces applied to the FLGR in the NEM switching process. (b) Schematic diagrams which show the proposed switching mechanism of the NEM device based on FLGRs.

the long, narrow nanogap gives rise to a large F_a, thus the device shows a good bias response. In addition to F_a, a van der Waals force (F_v) also acts on and deflects the edges when they are close to each other. Counteracting F_a and F_v is elastic repulsive force (F_e), which tries to separate the edges to restore their original positions. The equilibrium position of the edges is defined by the balance of these forces (Figure 9a), and F_a impulses the switching process. Above V_t, a large F_a deflects the edges and causes them make electrical contact with each other. If one point is in contact, an "ON" state is established. However, at the bias higher than the breakdown voltage, the device will return to the "OFF" state, as no available contact can be established at this bias due to the current breakdown. Below V_t, F_a and a small F_v cannot counteract F_e of the tensioned ribbon, thus the edges spring back to noncontact "OFF" state. Due to the capacitive charging effect, a small current can be observed in this state. FLGRs, produced here, are ideal for use of the NEM devices, as it has not only a good conductivity and flexibility but also a sufficient bending rigidity for the switching operation. As reported by Poot et al.,[16] the bending rigidity shows a strong thickness dependence, thus the few-layer graphene provides a larger bending rigidity than single-layer graphene, which gives rise to an appropriate F_e for the NEM operation.

Moreover, we fabricated logic circuits based on the NEM switches. As an example, a simple logic OR gate device is fabricated by connecting two NEM switches in parallel (Figure 10a). In electronics, data processing requires the encoding of information in electrical signals in the form of binary digits, thus a threshold value and a logic convention are established for each signal.[36] In our cases, the signal is encoded by a positive logic convention and a threshold value of 7 V, thus a voltage

(36) Mitchell, R. J. *Microprocessor System: An Introduction*; Macmillan: London, 1995.

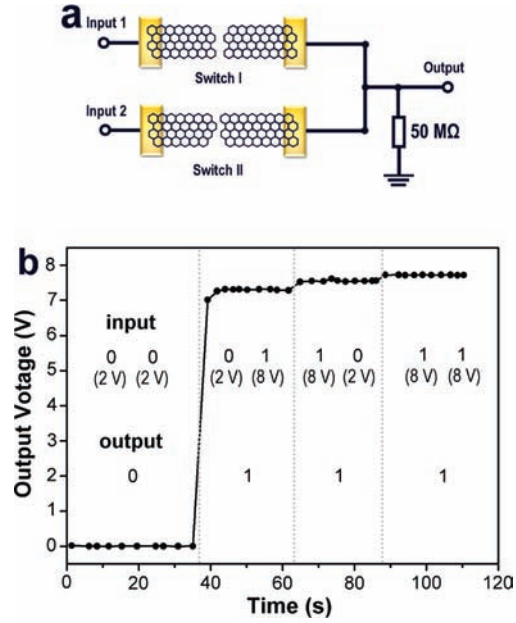

Figure 10. (a) Schematic of the electronic circuit of a logic OR gate. (b) Output voltage of the logic OR gate for the four possible inputs: (0,0), (0,1), (1,0), (1,1) and the truth table.

above 7 V represents a logical "1", while a voltage below represents a logical "0". Figure 10b shows the output−input voltage response and the experimental truth table of this device. When either or both of the inputs are logical "1", the output is logical "1". The output is logical "0" only when both inputs are logical "0", as neither switches are open.

4. Conclusions

In conclusion, we developed a template CVD method to produce FLGRs. In the process, the ZnS ribbons serve as the template and provide large surface area for the graphene growth, thus scalable samples of FLGRs with well controlled morphologies are produced on Si substrates, and it can be further scaled up if a larger substrate is used. Besides the ZnS ribbons, it also has the potential to use various architectures of other materials as the template, resulting in graphenes with many other morphologies. As an application, we fabricate reversible NEM switches by using FLGRs and find that the few-layer graphene is an ideal material for applications in NEM. Moreover, we also fabricate a logic OR gate based on these NEM switches. This work opens up a feasible avenue for controllable and scalable production of graphene and provides an application of graphene in NEM, thus it would be valuable for both the scientific studies and the practical applications of graphene.

Acknowledgment. This work was supported by the National Natural Science Foundation of China (60736004, 60671047, 50673093, 60736004, 20825208), the Major State Basic Research Development Program (2006CB806200, 2006CB932100), the National High-Tech Research Development Program of China (2008AA03Z101), and the Chinese Academy of Sciences.

Supporting Information Available: Complete refs 4, 19a, 23, and 26; supporting figures (Figure S1−S9); detailed description of the preparation of ZnS ribbons; and detailed description of production of graphene membrane on ZnS films. This material is available free of charge via the Internet at http://pubs.acs.org.

JA903092K